# The insect somatostatin pathway gates vitellogenesis progression during reproductive maturation and the post-mating response

**Chen Zhang**
Gwangju Institute of Science and Technology
**Crisalejandra Rivera Pérez**
Consejo Nacional de Ciencia y Tecnología, Centro de Investigaciones Biológicas del Noroeste
**Fernando Noriega**
Florida International University
**Young Joon Kim** ( kimyj@gist.ac.kr )
Gwangju Institute of Science and Technology https://orcid.org/0000-0002-7990-754X

**Article**

**Keywords:** fruit fly, Drosophila melanogaster, sexual maturation, post-mating response.

**Posted Date:** April 14th, 2021

**DOI:** https://doi.org/10.21203/rs.3.rs-381466/v1



**Version of Record:** A version of this preprint was published at Nature Communications on February 18th, 2022. See the published version at https://doi.org/10.1038/s41467-022-28592-2.

# Abstract

Oogenesis is closely linked with reproductive maturation and mating status in females. In the fruit fly *Drosophila melanogaster*, vitellogenesis (yolk accumulation) is an important control point for oogenesis. Vitellogenesis begins upon eclosion and continues through the process of sexual maturation. Upon reaching sexual maturity, vitellogenesis is placed on hold until it is induced again by a mating signal. In flies, this mating signal is sex peptide (SP), a seminal substance that triggers robust egg-laying activity. However, the neural mechanisms that gate vitellogenesis in response to developmental and reproductive signals remain unclear. Here, we have identified a pair of thoracic ganglion neurons that produce the neuropeptide allatostatin C (*AstC-mTh*). AstC inhibits the biogenesis of juvenile hormone (JH), a key endocrine stimulator of vitellogenesis. Our genetic evidence indicates that *AstC-mTh* neurons gate both the initiation of vitellogenesis that occurs post-eclosion and its re-initiation post-mating. During sexual maturation, which takes place shortly after eclosion, *AstC-mTh* neurons are activated by excitatory inputs from SP abdominal ganglion (SAG) neurons. In mature virgin females, high sustained activity of SAG neurons seems to shut off vitellogenesis via continuous activation of the *AstC-mTh* neurons. Upon mating, however, SP inhibits SAG neurons, leading to *AstC-mTh* neuronal activation. As a result, the inhibition of the CA maintained by the AstC neurons is lifted. This permit both JH biosynthesis and the progression of vitellogenesis in mated females. Our work has uncovered a central neural circuit that gates the progression of oogenesis during sexual maturation and the post-mating response.


# Introduction

In *D. melanogaster*, ovary morphogenesis begins in the third larval instar and is completed within 48 hours after pupariation[1]. The ovary contains about 16 ovarioles, each of which represents an independent egg assembly line with progressively developing follicles (egg chambers). This assembly line begins with dividing germline stem cells (GSC) at one end and ends with mature eggs at the other. During oogenesis, a GSC divides asymmetrically to produce a daughter GSC and a cystoblast. The cystoblast subsequently divides four times to produce a cystocyte complex comprising one oocyte and 15 nurse cells. A layer of follicular epithelial cells adheres to and surrounds the oocyte-nurse cell complex to produce a stage 1 follicle. During maturation, follicles undergo sequential transitions from pre-vitellogenesis (stages 1–7) to vitellogenesis (i.e., yolk accumulation) (stages 8–14). In *D. melanogaster*, females molt into the adult stage (i.e., undergo eclosion) with ovaries that lack vitellogenic follicles [2]. Vitellogenesis begins after eclosion and continues throughout reproductive maturation.

Vitellogenesis initiation is an important control point in oogenesis that integrates hormonal cues to match the female physiological conditions (i.e., nutrition, mating status, etc). The major gonadotropic hormones in *D. melanogaster* are juvenile hormone (JH) and the insect steroid hormones referred to as ecdysteroids[3]. Ecdysteroids stimulate yolk protein (YP) synthesis in the fat body[4], while JH stimulates the synthesis and uptake of YP by the ovary[4,5]. Thus, JH is essential for the continuing development of vitellogenic follicles past stages 8 and 9. As female fly complete reproductive maturation, JH levels fall

gradually and vitellogenesis ceases. Later, mating once more stimulates the oogenesis that is required to sustain robust egg-laying activity in mated females. In *D. melanogaster*, a male-derived seminal fluid protein called sex peptide (SP) elicits oogenesis progression[6]. SP induces GSC proliferation by stimulating the biosynthesis of ecdysteroids[7]. The mechanism by which SP regulates JH biosynthesis and vitellogenesis, however, remains unclear.

The sperm-containing seminal fluid males transfer to females during copulation is composed of a wide range of chemical substances[8]. Not only does seminal fluid provide a supportive milieu for sperm survival, it also modifies the physiology and behavior of recipient females to maximize sperm fertility. SP is the most well-studied seminal fluid substance in *D. melanogaster*. SP is a 36-mer peptide produced by the male accessory gland[9] and attached to sperm tails. SP is transferred to females and stored in the female sperm storage organs[10]. Because it is released continuously from sperm by proteolysis of a trypsin-like cleavage site, it can sustain the post-mating state as long as sperm remains in the sperm storage organs (typically about a week). SP acts through SP receptor (SPR)—a G-protein coupled receptor that functions via Gαi or Gαo—to silence SPR-expressing peripheral sensory neurons (SPSN). SPSNs innervate the lumen of the uterus and send axonal processes into the tip of the abdominal ganglion, relaying the SP signal to Mip-vAL and SAG neurons. Mip-vAL neurons connect SPSNs and SAG neurons in the abdominal ganglion[11]. SAG neurons project to the dorsal protocerebrum in the brain and regulate SP-associated behaviors and physiological responses. These include the suppression of mating receptivity[12], vaginal plate opening[13], stimulation of oviposition[14], increasing salt preference[15], and reduced siesta sleep[16]. Thus, the SP signal seems to diverge after passing through the SAG neurons to regulate a multitude of post-mating behaviors and physiological changes. The recent discovery of the neural pathways that implicate SAG neurons in oviposition and mating receptivity (i.e., vaginal plate opening) support this notion[13,14]. Still, the circuits downstream of the SAG neurons that regulate vitellogenesis remain unknown.

In this study, we identified two pairs of allatostatin C (AstC)-producing thoracic ganglion neurons (*AstC-mTh*) that link SAG neurons with JH biosynthesis and vitellogenesis initiation, not only in mated females, but also in young virgin females during reproductive maturation. AstC was first identified in the hawkmoth *Manduca sexta* based on its “allatostatic” activity (i.e., inhibition of JH biosynthesis) against the JH-producing endocrine organ referred to as the corpora allata (CA)[17]. An allatostatic function was also ascribed to AstC in *D. melanogaster* when one group found that knockdown of either AstC or AstC receptors increases JH-III levels[18]. In this study, we found that SAG neurons function upstream of *AstC-mTh* neurons, which secrete AstC and inhibit JH biosynthesis in the CA via AstC receptors (star1 and AstC-R2). As young virgin female complete reproductive maturation, SAG neuron activity rises, augmenting the AstC-induced inhibition of the CA. In mated females, the SP signal attenuates SAG neuron activity and, in turn, the secretion of AstC from AstC-mTh neurons. This reduces AstC-induced inhibition of the CA, eventually permitting JH biosynthesis and vitellogenic oocyte development.

# Results

## AstC gates vitellogenesis during reproductive maturation

In *D. melanogaster*, adult females emerge with ovaries lacking vitellogenic follicles (i.e., follicles older than stage 8). To better understand the progression of vitellogenesis that takes place during reproductive maturation, we examined the ovaries of virgin females, counting early (stages 8–11) and late vitellogenic follicles (stages 12–14) separately over 5 days after eclosion. We found control ovaries contained vitellogenic follicles as early as 12 hours post-eclosion (white bar in Fig. 1a). Early vitellogenic follicles accumulated quickly and reached maximum numbers (17 ± 3 oocytes per female) within 24 hours. They then remained elevated for an additional 24 hours before declining again and reaching a lower basal level thereafter. Later-stage vitellogenic follicles (stages 12–14) began to appear 24 hours after eclosion. They then continued to increase over 3–4 days before reaching a maximum. Thus, vitellogenesis during reproductive maturation seems to progress in two distinct phases. The initial phase, characterized by a rapid accumulation of early vitellogenic follicles, begins soon after eclosion and lasts 48 hours. In the subsequent phase, vitellogenesis initiation slows down until coming to an end 72 hours after eclosion. This maintains the number of early vitellogenic follicles at roughly 31–55% of its peak.

Considering the role of AstC in generating the circadian vitellogenesis rhythm[19], we examined post-eclosion vitellogenesis in virgin females lacking a functional *AstC* allele. As with the wild-type controls described above, the ovaries of AstC-deficient ($AstC^{1}/AstC^{1}$) females contained no vitellogenic follicles when examined immediately after eclosion. Twelve hours later, however, AstC-deficient ovaries produced considerably more early-stage follicles (10 ± 1 follicles per female) than controls (3 ± 1 follicles per female). This difference between the two groups reached statistical significance at both 12 and 24 hours after eclosion, but not at 48 hours after eclosion or thereafter (Fig. 1a). Thus, AstC seems to delay the initial phase of vitellogenesis post-eclosion.

Next, we restored AstC expression in *AstC-Gal4* cells and again examined vitellogenesis progression post-eclosion. As expected, we found restoration of AstC in *AstC-Gal4* cells reduced the number of early-stage vitellogenic oocytes to control levels (compare the white and blue bars in Fig. 1a). *AstC-Gal4* drives expression in many central nervous system (CNS) neurons[19]. Among these, six pairs of neurons referred to as circadian dorsal neuron 1 (AstC-DN1) are involved in vitellogenesis initiation, specifically with its circadian rhythm. Unlike *AstC-Gal4*, however, restoration of AstC expression in AstC-DN1 alone failed to restore the number of early vitellogenic oocytes to control levels (Fig. S1a). Thus, AstC-DN1 is unlikely involved in the vitellogenesis associated with reproductive maturation.

## AstC Neurons That Function During Reproductive Maturation

Consistent with an inhibitory role for the AstC neurons that arrest vitellogenesis associated with reproductive maturation, activation of the *AstC-Gal4* neurons of virgin females for three days shortly after eclosion significantly reduces total oogenesis[19]. In an attempt to map the responsible AstC neurons, we restricted the expression of the *AstC-Gal4* driver to distinct subsets of neurons by preparing five additional Gal4 transgenes (*AstC-A*, *AstC-B*, *AstC-C*, *AstC-D*, and *AstC-E*), each carrying a ~ 1-kb genomic fragment that together tile the 5'-upstream cis-regulatory region of *AstC* used to generate the original *AstC-Gal4*

(Fig. 1b). We then used these additional Gal4 drivers to drive expression of the warmth-activated cation channel dTrpA1, thus permitting the specific activation of subsets of the neurons targeted by the original AstC-Gal4 transgene. Among these five new GAL4 lines, *AstC-D-Gal4* activation led to a significant reduction in total oogenesis. Females carrying both *AstC-D-Gal4 and UAS-dTrpA1* produced ~ 50% fewer mature eggs at 30°C than control females carrying *AstC-D-Gal4* alone (Fig. 1c).

Next, we further examined the role *AstC-D-Gal4* neurons play in vitellogenesis by driving the expression of the inwardly-rectifying potassium channel Kir2.1[20] or temperature-sensitive dynamin mutant *shibire* ($Shi^{ts}$)[21], and counting the number of early and late vitellogenic follicles at 12 and 24 hours after eclosion. Remarkably, we found silencing *AstC-D-Gal4* neurons produced a phenocopy of AstC deficiency, leading young virgin females to produce more early-stage vitellogenic follicles (stages 8–11) than controls (Fig. 1d; Fig. S1b). This is precisely what would be expected if these are indeed the AstC neurons of interest—negative regulators of the vitellogenesis associated with reproductive maturation. Thus, we next asked whether the *AstC* gene is required for the oogenesis inhibition induced by *AstC-D-Gal4* neuron activation. Indeed, *AstC-D-Gal4* neuron activation failed to reduce total oogenesis in females lacking a functional *AstC* allele (Fig. 1e). Moreover, we confirmed that restoring AstC expression only in *AstC-D-Gal4* neurons can rescue vitellogenesis in AstC-deficient females to wild-type levels (Fig. 1f). On the strength of these data, we conclude that *AstC-D-Gal4* targets a subset of AstC neurons that gates the vitellogenesis associated reproductive maturation.

## Identification of *AstC-mTh* neurons

To further restrict *AstC-D-Gal4* activity to a smaller group of cells, we employed the split-Gal4 system[22]. Genomic DNA fragments used to generate *AstC-Gal4* and *AstC-D-Gal4* were fused with the Gal4 DNA-binding (DBD) and transcription activation domains (AD), respectively, and combined to produce *AstC-D-split-Gal4* (i.e., *AstC-Gal4DBD; AstC-D-Gal4AD*). We found that thermal activation of *AstC-D-split-Gal4* neurons suppressed total oogenesis to a level comparable to that of *AstC-D-Gal4* neuron activation (i.e., compare Fig. 2a with Fig. 1e). Moreover, when we used *AstC-D-split-Gal4* to drive expression of *AstC-RNAi*, we observed a nearly complete de-repression of the oogenesis inhibition caused by *AstC-D-split-Gal4* neuron activation (Fig. 2a). Of note, expression of *AstC-RNAi* in *AstC-D-split-Gal4* neurons also led to a nearly complete loss of anti-AstC expression in the ventral nerve cord (VNC) and dorsal subesophageal zone (SEZ) (red arrows in Fig. S2a).

When we examined the CNS of flies expressing myr-EGFP in *AstC-D-split-Gal4* neurons, we found 40 cells with neuron-like morphology (Fig. 2b, c). Of these cells, 6 in the brain and 8 in the ventral nerve cord (VNC) were also positive for anti-AstC (orange circles in Fig. 2c). To visualize and examine the function of *AstC-D-split-Gal4* neurons in the brain, we combined *AstC-D-split-Gal4* with $Otd^{FLP}$ [23,24]. Unlike the larger population of *AstC-D-split-Gal4* neurons, $Otd^{FLP}$-positive brain neurons had a limited impact on total oogenesis (Fig. 2d, Fig. S2b). This suggests the *AstC-D-split-Gal4* neurons in the brain are not important for this particular outcome.

Considering the fact that the silencing of AstC neurons (i.e., *AstC-D-Gal4* neurons) seems to expedite post-eclosion vitellogenesis by ~ 12 hours, AstC neurons associated with reproductive maturation should already be active prior to eclosion. Thus, we monitored neural activity in *AstC-D-split-Gal4* neurons using TRIC (i.e., transcriptional reporter of intracellular $Ca^{2+}$), which increases GFP expression in proportion to $[Ca^{2+}]_i$ [25]. We observed a robust TRIC signal exclusively in a pair of AstC neurons in the mesothoracic ganglion (hereafter referred to as *AstC-mTh* neurons) (arrows in Fig. 2e), which remained unchanged in all examined time points from − 1 to 3 days post-eclosion (Fig. S2c, Fig. S2d). At low frequency (~ 10%), we observed TRIC labeling of only a single *AstC-mTh* neuron, revealing its anatomy at single-cell resolution (Fig. 2f). This single *AstC-mTh* neuron, with its soma located in the mesothoracic ganglion, extensively innervates the dorsal regions of the prothoracic and mesothoracic ganglia and sends an ascending projection that arborizes around the SEZ and inferior dorsal brain. The descending processes from this *AstC-mTh* neuron do not project beyond the mesothoracic ganglion to the abdominal ganglion.

Next, by driving the expression of the post-synaptic marker DenMark[26] and the pre-synaptic marker Syt-GFP[27] with *AstC-D-split-Gal4*, we sought to identify, respectively, the inputs and outputs of the *AstC-mTh* neurons. We observed staining of Syt-GFP indicating the outputs of *AstC-mTh* in the dorso-lateral mesothoracic ganglion, SEZ, and inferior dorsal regions of the brain (Fig. 2g). DenMark staining was evident in somas, medially running along the mesothoracic ganglion to the SEZ, indicating these as *AstC-mTh* neuron inputs (Fig. 2h). The *AstC-mTh* neurons and their ascending projection that arborizes the SEZ were evident in both sexes (Fig. 2i, 2j).

### *AstC-mTh* neurons inhibit JH biosynthesis in the CA

AstC was initially identified due to its direct allatostatic actions on the CA of the hawkmoth *M. sexta*[17]. This is why we next asked whether *AstC-mTh* neurons inhibit JH production. We measured JH-III levels from female whole-body extracts (Fig. S3). We found that $w^{1118}$ females produced ~ 10 times higher JH-III levels on the first day post-eclosion (day 1) than during the pupal S8 stage (day − 2). Next, we subjected females expressing dTrpA1 in *AstC-D-Gal4* neurons to thermal activation for three days beginning at pupal stage S8 and then measured JH-III levels on day 1 post-eclosion. Indeed, we found thermal activation of *AstC-D-Gal4* neurons produced a significant suppression of JH production. To further understand the role of *AstC-mTh* neurons modulating JH titers, we evaluated JH signaling by quantifying mRNA levels of Krüppel homolog 1 (Kr-h1), a transcriptional target of JH signaling[28]. In our previous study, we confirmed that Kr-h1 mRNA levels mirror JH levels with good sensitivity and fidelity[19]. When we activated *AstC-D-Gal4* neurons, we observed a significant reduction in Kr-h1 transcript, to a level approximately 75% of that of the control group (Fig. 3a). To provide further evidence, we asked how the JH mimic methoprene affects vitellogenesis in the presence of *AstC-D-Gal4* neuron activation. We found females treated with methoprene showed a significant de-repression of the inhibition of total oogenesis induced by a 3-day thermal activation of *AstC-D-Gal4* neurons (Fig. 3b).

Because activation of *AstC-mTh* neurons seems to inhibit JH biosynthesis, we next tested the possibility that the JH-producing CA receives the AstC signal directly. The *Drosophila* genome contains two AstC-receptor genes, *star1* (aka *AstC-R1*) and *AlCR2* (aka *AstC-R2*), both of which encode G-protein coupled receptors highly sensitive to and selective for AstC[29]. We examined the CA in *AstC-R1-Gal4* or *AstC-R2-Gal4* females, each of which carries an extra exon of the TA-Gal4 transgene in their respective receptor loci[19,30]. Juvenile Hormone Acid O-Methyl Transferase (JHAMT) is the rate-limiting enzyme for JH production, and it is expressed exclusively in the CA[31]. We found the CA labeled by anti-JHAMT were also positive for both *AstC-R1-Gal4* and *AstC-R2-Gal4* (Fig. 3c, d). Finally, when we knocked down each receptor in the CA one at a time, we found depletion of each receptor accelerated and increased vitellogenesis in young virgin females, recapitulating the phenotype we observed in those with AstC deficiency or *AstC-mTh* neuronal silencing (Fig. 3e). When we used *JHAMT-Gal4* to drive over-expression of either AstC-R1 or -R2 in the CA, we saw a limited effect on total oogenesis, as measured by the number of mature stage 14 eggs. But simultaneous expression of both AstC-R1 and -R2 in the CA significantly reduced total oogenesis (Fig. 3f). Together, these results suggest the CA is indeed exposed to AstC during reproductive maturation.

### *AstC-mTh* neurons inhibits the CA likely via a hormonal route

To determine whether *AstC-mTh* neurons innervate the CA directly, we expressed *UAS-myr-EGFP* in *AstC-D-split-Gal4* neurons and could not detect GFP signal around the CA of females (Fig. S4a). Thus, any communication taking place between *AstC-mTh* neurons and the CA is unlikely occurring via a neuronal route. We did, however, notice *AstC-mTh* neurons projecting to the dorsomedial SEZ where the aorta contacts the brain (arrow in Fig. 2f and Fig. 2g). This is reminiscent of the SEZ innervation of insulin producing cells (IPCs), neuroendocrine cells that also stimulate JH biosynthesis[32,33]. In a previous study, we found that the activation of another subset of AstC neurons (i.e., *AstC-DN1p* neurons) inhibits JH biosynthesis by suppressing the secretory activity of the IPCs, causing a significant increase in anti-Dilp2 staining as Dilp2 accumulates[19]. For this reason, we tested the possibility that *AstC-mTh* neuron activation inhibits IPC activity, affecting JH biosynthesis indirectly. Unlike *AstC-DN1p* neurons, however, thermal activation of *AstC-mTh* neurons had a limited impact on anti-Dilp2 levels in IPCs (Fig. S5a). Inhibition of IPCs or insulin signaling during development typically leads to adults with small body size. And while constitutive activation of *AstC-DN1p* neurons does indeed produce adults with small body size[19], similar activation of *AstC-mTh* neurons does not measurably affect adult body size (Fig. S5b). Thus, we have concluded that unlike *AstC-DN1p* neurons, *AstC-mTh* neurons do not function through the IPCs. Considering the absence of AstC processes innervating the CA, the most parsimonious hypothesis is that *AstC-mTh* neurons, like IPCs, also secrete their contents (i.e., AstC) into the circulation to suppress JH biosynthesis in the CA via a hormonal route.

### *AstC-mTh* neurons play a role in post-mating vitellogenesis

In *D. melanogaster*, the mating signal SP stimulates oogenesis progression, specifically vitellogenesis[6]. We reasoned that SP likely does so by inhibiting *AstC-mTh* neurons, relieving AstC-mediated inhibition of

the CA. To explore this hypothesis, we first evaluated the activity of *AstC-D-split-Gal4* neurons in females before and after mating using TRIC. *AstC-mTh* neurons in 4-day-old virgin females show strong TRIC signal (Fig. 4a, b), but this is significantly down-regulated within 48 hours after mating with control males, but not after mating with SP-less males (Fig. 4c).

Because SP appears to inhibit the activity of *AstC-mTh* neurons, we wanted to determine whether SP stimulates vitellogenesis via the *AstC-mTh* neurons. We therefore counted vitellogenic follicles (stages 8–14) and oviposited eggs every four hours after mating for two days (Fig. S6). In control $w^{1118}$ females, we first observed oviposition activity 4 hours after mating, leading to a concomitant reduction in stage 14 eggs. We were unable to observe mating-induced vitellogenesis until 12 hours post-mating, when the number of stage 10 follicles rose compared with virgin controls. Of note, we did not observe any measurable increase in follicles of other stages, whereas stage 10 follicles remained consistently elevated until the end of the experiment. Since it takes ~ 12 hours for pre-vitellogenic stage 7 follicles to become stage 10 follicles[34], the increase in stage 10 follicles observed 12 hours post-mating likely reflects mating-induced vitellogenesis commencing almost immediately after mating. Consistent with this interpretation, females mated with SP-less males showed no increase in stage 10 follicles, as examined 24 hours post-mating (Fig. S6g).

Next, we asked whether *AstC-mTh* neurons control mating-induced vitellogenesis. Females expressing dTrpA1 in *AstC-mTh* neurons (i.e., *AstC-D-split-Gal4* neurons) were incubated at 30°C for 24 hours after mating. We assumed that thermal activation of *AstC-mTh* neurons would override SP-induced inhibition of *AstC-mTh* neurons, restoring virgin-like *AstC-mTh* activity. Indeed, thermal activation blocked mating-induced vitellogenesis, reducing stage 10 follicles by ~ 50% when compared with controls (Fig. 4d). We also expected *AstC-mTh* neuronal silencing would recapitulate mating-induced vitellogenesis even in virgin females. When we blocked the secretory activity of *AstC-mTh* neurons via expression of the $Shi^{ts}$, we were unable to observe any difference in the number of vitellogenic follicles (stages 8–14) in 4-day-old virgin females (Fig. 4e). Thus, we have concluded *AstC-mTh* neurons do not simulate vitellogenesis *per se*, but instead gate the vitellogenesis progression that seems to be stimulated by other mating-associated allatotropic factors.

*AstC-mTh* neurons are interneurons with neurites that innervate the CNS. Because SP inhibits *AstC-mTh* neurons in the same way it inhibits SAG neurons and other neural components of the SP response circuit[11,12], we wanted to determine whether *AstC-mTh* neurons are functionally linked with SAG neurons. Thus, we prepared female flies expressing TrpA1 in SAG neurons and incubated them at 30°C for 24 hours after mating. We expected thermal activation of SAG neurons to override their SP-induced inhibition, thus restoring virgin-like neural activity. Remarkably, we found thermal activation of SAG neurons precisely recapitulated the phenotype induced by thermal activation of *AstC-mTh* neurons we described above; it blocked mating-induced vitellogenesis and reduced the number of stage 10 follicles by ~ 50%. Unlike with *AstC-mTh* neurons, however, activation of SAG neurons also suppressed oviposition, increasing stage 14 eggs in the ovaries. Thus, SAG neurons modulate both vitellogenesis and oviposition, whereas *AstC-mTh* neurons gate vitellogenesis without affecting oviposition (Fig. 4f).

### The role of SAG neurons in vitellogenesis during reproductive maturation

Having shown that SAG neurons and *AstC-mTh* neurons are functional associated in mating-induced vitellogenesis, we wondered whether SAG neurons are also involved in vitellogenesis in young virgin females during reproductive maturation. When we suppressed SAG neuronal activity with Kir2.1 and examined vitellogenesis at 12 and 24 hours after eclosion, we found significantly elevated numbers of early vitellogenic follicles (stages 8–11) just like we observed in females with silenced *AstC-mTh* neurons (Fig. 5a). Next, we asked whether activation of SAG neurons during reproductive maturation suppresses vitellogenesis and reduces total oogenesis. We found thermal activation of SAG neurons for 3 days post-eclosion reduced the number of stage 14 eggs by ~ 50% (Fig. 5b).

We then wondered whether SAG neurons function through AstC or AstC-mTh neurons. In the absence of a functional AstC allele, thermal activation of SAG neurons failed to suppress total oogenesis (Fig. 5b). Having shown that AstC is required for the function of SAG neurons, we wondered whether *AstC-mTh* neurons also function downstream of SAG neurons. To test this hypothesis, we activated SAG neurons while also silencing *AstC-mTh* neurons with Kir2.1. As with AstC-deficiency, the silencing of *AstC-mTh* neurons also seemed to relieve the vitellogenesis blockade induced by SAG neuron activation, restoring total oogenesis to control levels (Fig. 5c). We then asked whether a JH mimic could override SAG neuron activation and restore total oogenesis to control levels. We found methoprene treatment reversed the vitellogenesis suppression imposed by SAG neuron activation and restored the number of stage 14 eggs to control levels (Fig. 5b). This result provided further evidence of a causal link between SAG neurons and the JH pathway. Finally, we examined SAG neuron activity during reproductive maturation using TRIC analysis (Fig. 5d). As expected, we found evidence of a gradual increase in SAG neural activity the first two days post-eclosion, reaching maximum activity on day 3 when the vitellogenesis associated with reproductive maturation ends (Fig. 1a).

### SAG neurons do not form conventional chemical synapses with *AstC-mTh* neurons

Having shown that *AstC-mTh* neurons function downstream of SAG neurons, we wondered how SAG neurons and *AstC-mTh* neurons interact with one another at the cellular level. By labeling the pre-synaptic terminals of SAG neurons with Syt-GFP, we determined that the SAG outputs arborize near *AstC-mTh* somas as well as in the mediodorsal SEZ where *AstC-mTh* neurons project and form extensive post-synaptic terminals (Fig. S7a). Thus, we further explored the possibility that SAG neurons form functional synapses with AstC-mTh neurons by adopting the *trans*-Tango technique, which visualizes functional post-synaptic neurons[35]. We found SAG neuron expression of *trans*-Tango labeled many post-synaptic neurons, primarily in the abdominal ganglion. But even after many attempts, we failed to detect *trans*-Tango activity in *AstC-mTh* neurons (Fig. S7b). Thus, it seems unlikely that SAG neurons form conventional chemical synapses with *AstC-mTH* neurons.

## Discussion

Oogenesis is energetically demanding and must be coordinated with ongoing developmental, physiological, and metabolic processes. Vitellogenesis initiation is a critical control point for oogenesis in *D. melanogaster*. In this species, vitellogenesis begins shortly after eclosion and continues through reproductive maturation, in which females prepare for mating and egg-laying. As females mature over two or three days, vitellogenesis ceases until mating stimulates it again to sustain egg-laying activity. The seminal substance SP acts as a mating signal, stimulating vitellogenesis, ovulation, and oviposition. In this study, we identified a pair of thoracic ganglion neurons (i.e., *AstC-mTh* neurons) that express the insect somatostatin AstC. We provide evidence that AstC from these neurons modulates vitellogenesis by gating two distinct episodes of JH biosynthesis, one stimulated by adult molting (i.e., eclosion) and the other stimulated by mating. We have also uncovered a functional link between *AstC-mTh* neurons and SAG neurons, which are a key component of the SP response circuit.

### *AstC-mTh* neurons delay reproductive maturation

In *D. melanogaster*, JH acts on the ovary to initiate vitellogenesis[36,37]. JH levels peak at eclosion (day 0) and decrease gradually over several days[38,39]. JH titer and therefore oogenesis progression are closely coupled to the endocrine events that induce eclosion in at least two dipteran species, *A. aegypti* and *D. melanogaster*[40,41]. Ecdysis triggering hormone (ETH), which induces molting behaviors (i.e., eclosion) in almost all insect species ever examined[42,43], also functions as a potent allatotropin. When a pharate adult female is ready to emerge from the pupal case, the endocrine Inka cells secrete ETH. ETH enters the circulation and acts hormonally on the CNS to trigger a sequence of stereotypic motor patterns that culminate in eclosion. When circulating ETH reaches the CA, it triggers the post-eclosion surge of JH. Considering the 28-hour delay required for previtellogenic stage 7 follicles to develop into stage 11 follicles, the ETH-induced JH surge at day 0 is likely responsible for the marked increase of early vitellogenic follicles (stages 8–11) detected at day 1. In this study, we found that AstC-deficiency in *AstC-mTh* neurons and silencing *AstC-mTh* neurons both advance vitellogenesis initiation by ~ 12 hours. This suggests AstC-deficiency must also advance the JH peak by ~ 12 hours, and that *AstC-mTh* neurons are involved in a temporal decoupling between endocrine events associated with eclosion and reproductive maturation. It is unclear why *Drosophila* has evolved a mechanism to delay reproductive maturation. In addition to vitellogenesis, JH also stimulates other processes associated with reproductive maturation, such as pheromone production and the development of mating receptivity[44]. In the wild, *D. melanogaster* males often wait for females to emerge from their pupal cases before forcefully mating with them[45,46]. We speculate a programmed delay in the processes required for developing attractiveness toward males and mating receptivity would contribute to female fitness by increasing the temporal window in which females can select the best available suitor. The time required for females to reach reproductive maturity varies across *Drosophila* species. For example, *D. pachea* females require weeks to become ready to mate, whereas *D. mettleir* females are ready to mate within hours of eclosion. Thus, a comparative analysis of AstC's role in programming the delays required for reproductive maturation across species would be of the great interest[47].

As with AstC-deficiency, SAG neuron silencing also advanced post-eclosion vitellogenesis by ~ 12 hours. In contrast, activation of SAG neurons during reproductive maturation (i.e., for 3 days post-eclosion) reduced oogenesis by ~ 50%, precisely phenocopying *AstC-mTh* neuron activation. We also found *AstC-mTh* neuron silencing blocks the oogenesis-suppressing effect of SAG neuron activation. This epistatic relationship between SAG neurons and *AstC-mTh* neurons strongly supports the hypothesis that *AstC-mTh* neurons function downstream of SAG neurons. Using the TRIC technique, we found a gradual increase in intracellular $Ca^{2+}$ in the SAG neurons over the 3 days following eclosion, indicating increased activity. This is consistent with the significant levels of spontaneous firing observed in patch recordings from the SAG neurons of 4–5-day-old virgin females[12]. We propose that as females undergo reproductive maturation, SAG neurons augment the excitatory inputs into *AstC-mTh* neurons, driving them to secrete more AstC and cause further inhibition of JH biosynthesis. Unlike what we observed with the SAG neurons, however, we did not see a progressive increase in TRIC staining of *AstC-mTh* neurons. But the TRIC staining we observed was so strong that it labeled the entire neuronal arbor of each *AstC-mTh* neuron. This suggests that a ceiling effect may have masked any further increase in TRIC activity associated with reproductive maturation.

Although we found AstC-deficiency significantly advanced vitellogenesis, it had a limited effect on total oogenesis in virgin females. This is probably because virgin females have limited pre-vitellogenic follicles that can enter vitellogenesis. Consistent with this interpretation, JH has no effect on GSC proliferation[7]. SP stimulates the ovary to produce ecdysteroids, which in turn, stimulate GSC proliferation and presumably pre-vitellogenic follicles. Moreover, there are additional control points and feedback mechanisms that regulate oogenesis progression. For example, ovulation seems to stimulate oocyte maturation. In the absence of ovulation, each ovariole accumulates no more than two or three mature oocytes. Thus, future studies should address whether ovulation modulates the activity of *AstC-mTh* neurons to stimulate JH production and vitellogenesis progression.

### *AstC-mTh* neurons in mating-induced vitellogenesis

An *ex vivo* analysis found that synthetic SP can induce JHB3 biosynthesis in isolated CA from 3–4-day-old virgin females[48]. Subsequently, SP was implicated in mating-induced vitellogenesis, which was characterized by a pronounced increase of vitellogenic stage 10 follicles[6]. In this study, we confirmed the stimulatory role of SP in mating-induced vitellogenesis by repeating the previous observation in the $w^{1118}$ background, from which most of the fly stocks used in this study were derived (Fig. S6). When SP from the male ejaculate was detected in the hemolymph of mated females, it was proposed to enter the circulation and hormonally stimulate the CA[49]. More recent studies since the discovery of SPR, however, have suggested SP acts mainly through neuronal pathways comprising SPSN neurons, Mip-vAL neurons, SAG neurons, and the pC1 neurons[11,12,14]. Of particular note, targeted expression of membrane-tethered SP (mSP) in uterine SPR neurons (i.e., SPSN neurons) induces virgin females to lay a large number of unfertilized eggs[50,51]. In other words, when mSP can activate SPR only in the neurons that express it without entering circulation, virgin female egg-laying was found to resemble that of mated females. Thus,

it is likely that mSP stimulates vitellogenesis exclusively through a neuronal route through the SPSN neurons. Furthermore, electric silencing of either SPSN neurons or SAG neurons (i.e., both mimicking SPR activation) also stimulates robust egg-laying in virgin females at a level comparable to that of mated females[12]. The silencing of *AstC-mTh* neurons, however, failed to stimulate vitellogenesis in virgin females. Moreover, the activation of SAG neurons or *AstC-mTh* neurons led to a significant ~ 50% reduction in post-mating vitellogenesis. This means it is much more likely that mating-induced vitellogenesis is regulated by allatotropic signals under the control of the neuronal SP response pathway. For example, SP induces 20E biosynthesis via the neuronal SP response pathway[7]. This, in turn, activates ETH expression and secretion from adult Inka cells[41]. It remains unclear, however, whether mating or SP causes ETH secretion. Alternatively, yet not mutually exclusively, SP circulating in post-mating females may also play a role in stimulating JH biosynthesis, as previously proposed[48]. In other insect species, such as the noctuid moth *Spodoptera frugiperda* and the mosquito *A. aegypti*, mating-induced vitellogenesis also seems to be induced at least in part by JH transferred in the male ejaculate[52,53].

Unlike the SAG neurons, which suppress egg-laying activity, *AstC-mTh* neurons have limited impact on egg-laying *per se*. Egg-laying is the outcome of a coordinated array of reproductive processes, such as oogenesis (including vitellogenesis), ovulation, and oviposition. All of these processes are triggered by the neuronal SP pathway. For example, the neural circuit that links SAG neurons and oviposition behavior was recently discovered[14]. Activation of these neurons stimulates oviposition only in mated females, not virgin females. This is likely because this circuit is specialized for oviposition and can only function after oogenesis and ovulation. Our work establishes a novel and distinct branch of the neuronal SP pathway that is specialized exclusively for vitellogenesis.

### A source of hormonal AstC that acts directly on the CA

Since Kramer et al. (1991)[17] discovered AstC in the hawkmoth *M. sexta* and reported that it inhibits JH biosynthesis in isolated CAs, several subsequent studies implicated AstC in the regulation of biological processes as diverse as circadian rhythmicity, nociception and immunity in *Drosophila*[19,54,55]. AstC is expressed in a relatively large number of cells in the brain and gut, consistent with its functional pleiotropism. We found recently that AstC in six pairs of DN1p clock neurons in the brain generate the circadian vitellogenesis rhythm in mated females by rhythmically inhibiting the secretion of the insulin-like peptides that stimulate JH biosynthesis. In this study, we propose that *AstC-mTh* neurons are a source of AstC that circulates in the hemolymph to regulate JH biosynthesis associated with reproductive maturation and the post-mating response. We have presented two major lines of evidence. First, *AstC-mTh* neurons, with their somas in the mesothoracic ganglion, project into the dorsal region of the brain's SEZ. The SEZ is also innervated extensively by other neurosecretory neurons such as the IPCs. This anatomical feature suggests *AstC-mTh* neurons are neurosecretory, secreting their contents into the hemolymph. This would allow AstC to travel outside the CNS to the CA, which expresses two highly sensitive and selective GPCR-type AstC receptors (i.e., star1 and AstC-R2). In a second, more important line of evidence, we found knockdown of either of these receptors precisely recapitulated the 12 hour-

advance of vitellogenesis initiation that occurs in females with AstC-mTh neurons that lack AstC or that are silenced by Kir2.1.

### A potential link between *AstC-mTh* neurons and post-mating immune responses

In *D. melanogaster*, mating stimulates the innate immune system and induces the production of diverse antimicrobial peptides (AMP) including Metchnikowin, Diptericin, and Drosomycin, etc.[56]. As with other aspects of the post-mating response, SP is responsible for post-mating AMP induction. Females that mate with males lacking SP do not produce AMPs upon mating, and females that express SP ectopically and constitutively in the fat body produce AMP regardless of their mating status. Genetic evidence suggests SP induces AMP production via the Toll and Imd pathways. Interestingly, AstC was recently found to have an immunosuppressive function, dampening the Imd pathway[54]. Thus, our finding that SP reduces AstC secretion from *AstC-mTh* neurons offers an additional and indirect route by which SP boosts the innate immune response and AMP production. Nevertheless, SP likely stimulates the innate immune response via multiple pathways. This is because the SP domain that stimulates AMP production has been mapped to the N-terminal hydroxyproline-rich motifs, which is distinct from the C-terminal domain that activates the neuronal SP pathway via SPSN neurons and SAG neurons[57,58].

### Functional Parallels Between The AstC And SST Systems

Our work highlights striking conservation in the AstC/SST signaling system between insects and mammals. Not only are the mammalian somatostatin (SST) receptors (sstr1-5) orthologous to the *Drosophila* AstC receptors, but just as AstC inhibits the insect gonadotropin JH, SST inhibits the mammalian gonadotropins follicle-stimulating hormone (FSH) and leutenizing hormone (LH) via the hypothalamic neuropeptide gonadotropin releasing hormone (GnRH)[59]. In addition, at least one SSTR also functions as an immunosuppressor that inhibits inflammation[60] (see above).

In this study, we have shown that the insect SST/AstC pathway modulates JH biosynthesis during reproductive maturation and the post-mating response. JH levels are also linked to other processes associated with female reproduction, such somatic organ remodeling[61], pheromone production, and mating receptivity[44]. Moreover, *AstC-mTh* neurons are also present in males, in which JH regulates processes associated with male reproduction like sex pheromone detection[62] and male accessory gland development[63,64]. Future studies will be necessary to evaluate the roles of the *AstC-mTh* neurons in these diverse reproductive processes.

# Methods

**Fly stocks.** Flies were raised at 25°C and 60% humidity under a 12 h:12 h light:dark cycle on standard fly media. The stocks used in this study were previously reported or obtained from the Bloomington Drosophila Stock Center (BDSC), the Vienna Drosophila RNAi Center (VDRC), or the Korean Drosophila Resource Center (KDRC). These include *otd$^{FLP}$* [24], *UAS > stop > mCD8GFP* [65], *UAS > stop > dTrpA1* [66], *UAS-*

*dTrpA1*[67], *UAS-Shi*$^{ts}$[21], *SAG* (*VT50405*)*-Gal4*[12], *SAG-GAL4-split1-Gal4* (*VT50405-p65AD; VT7068-GAL4DBD*)[12], *SAG (VT50405)-LexA*[12], *nSynb-Gal4* carrying *UAS-Dicer2* and *UAS-mCD8-GFP* (gifts from Barry J.Dickson, Janelia Research Campus), y1 w* *P{UAS-myrGFP.QUAS-mtdTomato-3xHA}su(Hw)attP8; P{trans-Tango}attP40* (*trans*-Tango)[35], *AstC-R1-Gal4*[30], *AstC-R2-Gal4*[30], *JHAMT-Gal4*[31], SP-null males SP$^0$/Δ130[68], *CNMa-Gal4*[19] (KDRC stock number, 2002), *AstC*$^{1}$[19] (KDRC #2166), *UAS-Kir2.1* (*III*) (a gift from Jan Lab, University of California San Francisco), *UAS-Dicer2* (VDRC stock number, 24648), *UAS-mCD8::RFP*, *LexAop2-mCD8::GFP;nSyb-MI::nlsLexADBDo;UAS-p65AD::CaM* (BDSC stock number, 61679), *UAS-Syt-EGFP (BDSC #6926), UAS-DenMark* (BDSC #33061), *UAS-Kir2.1* (*II*) (BDSC #6596), *UAS-NaChBac* (BDSC #9466), *AstC-IR1 CG14919* (VDRC #13772), *AstC-R1-IR1 CG7285* (VDRC #13560), and *AstC-R2-IR1 CG13702* (BDSC #25940).

**Molecular biology.** The *AstC Gal4* lines were generated by dividing the 5'-upstream region of the AstC coding sequence into five ~ 1-kb tiling fragments. *AstC-A-Gal4 (II)*, *AstC-B-Gal4 (II)*, *AstC-C-Gal4 (II)*, *AstC-D-Gal4 (II)*, *AstC-D-Gal4AD (III), AstC-E-Gal4 (II)*, and *AstC-Gal4DBD (II)* were prepared in gateway vectors as previously described[69]. Each region was amplified via genomic DNA PCR, cloned into the pENTR vector (Invitrogen), and then recombined into pBPGal4.2::VP16Uw for Gal4, pBPp65AD::ZPUw for Gal4AD or pBPZpGAL4DBD::Uw for Gal4DBD. Each of the final plasmid DNAs was injected into w$^{1118}$ flies with specific landing sites on the second (VIE-72A) or third chromosome (VIE-49B) using the ΦC31 system. VIE-72A and VIE-29Ba were gifts from Barry J. Dickson, Janelia Research Campus. The genomic fragments and primer sequences used to generate these lines were as follows: *AstC-A-Gal4* (CACCtttccacgaatgctatgcaa, ggcgtcggtaaatgagaaaa), *AstC-B-Gal4* (CACCatttaccgacgccaatttca, gaaaagccaacagggtggta), *AstC-C-Gal4* (CACCtaccaccctgttggcttttc, aaacacggtcgcttaattcc), *AstC-D-Gal4* and *AstC-D-Gal4AD* (CACCaccgtgtttgccaggataat, tctgcatgcaacaggtaagc), *AstC-E-Gal4* (CACCtgttgcatgcagatgatt, tactcaccggtcctgtttcg), and *AstC-Gal4DBD (*CACCtttccacgaatgctatgcaa, tactcaccggtcctgtttcg). *UAS-AstC-R1* and *UAS-AstC-R2* were generated by cloning the NotI-AstC-ORF-KpnI fragment amplified from cDNA clone RH36507 (AY070699) into the SST13 vector and then inserting it into a specific site on the third chromosome (VIE-49B) using the ΦC31 system. The genomic fragments and primer sequences used to generate these lines were as follows: *UAS-AstC-R1* (*ttagcggcgcaccatgtttacgtggctgatgat, taatctagattacaatctgtctgctgca*) and *UAS-AstC-R2* (*aatgcggccgccaccatggaaggtggatggtgg, taatctagattataagtccgtgtggagcac*).

**Bioassays.** All assays were repeated on at least two different days. To evaluate vitellogenesis progression after eclosion and total oogenesis, freshly eclosed females were placed individually in vials for the indicated times or for three days and their ovaries were dissected in phosphate buffered saline (PBS). Vitellogenic follicles (stages 8–14) or mature eggs (stage 14) in both ovaries were counted under a stereomicroscope. The ovarioles were separated and the stages of the vitellogenic follicles were determined according to the method used by Jia et al.[34]. To evaluate mating-induced vitellogenesis progression, freshly eclosed females were aged in groups of 10, mated individually with *Canton-S* males or SP$^0$/Δ130 males in a 1-cm diameter chamber, and placed individually into vials for the indicated times or for 24 hours after mating. Vitellogenic follicles (stages 8–14) and oviposited eggs were counted. For

the thermal activation or silencing experiments, virgin or mated females kept individually in vials were transferred into a 30°C incubator for 24 hours immediately after copulation.

**Methoprene treatment.** Methoprene (Sigma-Aldrich, catalog number 40596-69-8) was dissolved in 95% ethanol (1 μg/μl) and added to warm fly food medium (in a liquid state) to produce a final concentration of 1.04 μl/ml[19,70]. Flies were fed this food containing 1.04 μl/ml methoprene or 1μl/ml 95% ethanol (vehicle control) individually for 3 days after eclosion.

**Immunohistochemistry.** Each fly CNS was dissected in PBS and fixed in 4% paraformaldehyde for 20–30 min at room temperature. After washing with PBST, the samples were then incubated with rabbit anti-GFP antibody (1:1000; Invitrogen, A11122), rabbit anti-AstC antibody (A gift from Dušan Žitňan, Slovak Academy of Sciences), rat anti-HA antibody (1:100; Roche, 11867423001)[71], rabbit anti-JHAMT (a gift from Ryusuke Niwa, University of Tsukuba), anti-Dilp2[72] (a gift from Yu Kweon from Korea Research Institute of Bioscience and Biotechnology) and mouse anti-nc82 antibody (1:50; Developmental Studies Hybridoma Bank) for 48 hours at 4°C. Alexa Fluor 488-labeled goat anti-rabbit IgG (1:1000; Invitrogen, A11008), Alexa Fluor 568 goat anti-mouse IgG (1:1000; Invitrogen, A11004), and Alexa Fluor 633 goat anti-rat IgG (1:500; Invitrogen, A21094) were used as secondary antibodies for 24 hours at 4°C. Confocal images were acquired with a Zeiss LSM700/Axiovert 200M (Zeiss) and processed in Image J[73].

To quantify anti-Dilp2 fluorescence, we used a method that was previously described[19]. The maximum intensity Z-projections of 15 consecutive confocal stacks (each 5 μm-thick) covering the somas of all 14 IPCs were merged in Image J. The relative anti-Dilp2 fluorescence intensity of each brain was calculated by setting the average of control brains (UAS-dTrpA1/+) (for Fig S5a) to 100%.

**TRIC analysis.** *AstC-D-split-Gal4* (*AstC-D-Gal4AD; AstC-Gal4DBD*) and *SAG-Gal4-split1* (*VT50405-p65AD; VT7068-GAL4DBD*) were crossed with the TRIC transgenes (*UAS-mCD8::RFP*, *LexAop2-mCD8::GFP;nSyb-MI::nlsLexADBDo;UAS-p65AD::CaM*; see above) to quantify post-mating changes in intracellular $Ca^{2+}$ in *AstC-mTh* neurons or SAG neurons. CNS tissues from 4-day-old virgin or mated females (2 days post-copulation) were processed as described above (see the Immunohistochemistry section), but not stained with anti-GFP. To quantify EGFP fluorescence, maximum intensity Z-projections of three confocal stacks (15 consecutive sections each 3.82 μm-thick) covering the entire soma of each neuron were merged in Image J. Then, the relative GFP intensity of each soma was calculated by setting the average of the somas in each group from virgin females to 100%.

**RT-qPCR.** Total RNA was extracted from whole adult female bodies ($n = 15$) using Trizol (Takara) according to the manufacturer's instructions. RNA (1 μg) was reverse transcribed with oligo (dT) primers (Promega) and Accupower RT premix (Bioneer). Quantitative RT-PCR reactions were performed in 10 μl reaction volumes using an IQTM5 real-time PCR detection system (Bio-rad) with the SYBR Premix Ex taq (Takara) according to the manufacturer's instructions. The gene specific primers for Rp49 and Kr-h1 were described previously[19]: Rp49 (forward/reverse, 5'- gacgcttcaagggacagtatctg/5'-aaacgcggttctgcatgag) and Kr-h1 (5'-gcccaaatatgaatccgctctacc/5'- gtcgtcgcccttgttcatgta).

**JH measurement.** For JH-III quantification, 10 pupa or adult female flies from the indicated genotypes and stages were homogenized with a glass musher and transfer to a silanized vial. Flies homogenates were processed by the method described by Bergot et al.[74] that includes an acetonitrile/pentane extraction and a $C_{18}$ solid-phase extraction cartridge purification. The recovered organic fraction was reduced to a volume of a 100 µl and the JH III epoxide ring was opened by the addition of 150 µl of sodium sulfide and incubation at 55°C for 30 min. Samples were then extracted with hexane; the recovered organic phase (~ 500 µl) was filtered with a Nalgene filter (0.2 µm nylon membrane, #176), dried under N2 and stored at -20°C until used. JH titers from these whole-body extracts were determined using a high performance liquid chromatography coupled to a fluorescent detector protocol (HPLC-FD)[75].

**Wing size measurement.** To measure fly wing size, we modified a method that was previously described[19]. Briefly, the right wings of 3-day-old female flies were dissected and mounted in 70% glycerol. Images of each wing were taken using a LEICA EZ4E and the LAS V4.10 program. The distance between wing landmarks #5 and #13 was measured with ImageJ and used as an indicator of wing size.

**Statistical analysis.** GraphPad Prism 5 (GraphPad) was used to analyze the data.

# Declarations

### Author contributions

Conceived and designed the experiment: C.Z. and Y.-J.K.; performed the experiments: C.Z.; analyzed the data: C.Z. and Y.-J.K.; contributed reagents and analysis: C.R.-P. and F.N.; wrote the manuscript: C.Z. and Y.-J.K.

### Acknowledgements

We thank S-I. Kang, H-S. Yoon, J. Mun and J. Song for excellent technical assistance, B. J. Dickson (Janelia Research Campus), D. Žitňan (Slovak Academy of Sciences) for reagents. This work was supported by the GIST Research Institute (GRI) grant funded by the GIST in 2021 and by Basic Science Research Programs (NRF-2015K2A1B8046794, NRF-2018R1A2A1A05079359, NRF-2019R1A4A1029724) through the National Research Foundation of Korea (NRF) funded by Ministry of Science and ICT, Republic of Korea. Stocks were obtained from the Korea *Drosophila* Resource Center (NRF-2017M3A9B8069650), the Bloomington *Drosophila* Stock Center and the Vienna *Drosophila* Resource Center.

# References

1. Lin, H. The stem-cell niche theory: Lessons from flies. *Nat. Rev. Genet.* **3**, 931–940 (2002).
2. Spradling, A. C. Developmental genetics of oogenesis. in *The Development of Drosophila melanogaster* (eds. Bate, M., & Martinez-Arias ,A.), vol. **1**, 1-70 (Cold Spring Harbor Laboratory Press, 1993).

3. Swevers, L., Raikhel, A. S., Sappington, T. W., Shirk, P. & Iatrou, K. Vitellogenesis and post-vitellogenic maturation of the insect ovarian follicle. in *Comprehensive Molecular Insect Science* (eds. Gilbert, L. I., & Iatrou, K.) vol. **1**, 87-155 (Elsevier, 2005).
4. Jowett, T. & Postlethwait, J. H. The regulation of yolk polypeptide synthesis in Drosophila ovaries and fat body by 20-hydroxyecdysone and a juvenile hormone analog. *Dev. Biol.* **80**, 225–234 (1980).
5. Postlethwait, J. H. & Handler, A. M. The roles of juvenile hormone and 20-hydroxy-ecdysone during vitellogenesis in isolated abdomens of Drosophila melanogaster. *J. Insect Physiol.* **25**, 455–460 (1979).
6. Soller, M., Bownes, M. & Kubli, E. Mating and sex peptide stimulate the accumulation of yolk in oocytes of Droosophila melanogaster. *Eur. J. Biochem.* **243**, 732-738 (1997).
7. Ameku, T. & Niwa, R. Mating-induced increase in germline stem cells via the neuroendocrine system in female Drosophila. *PLoS Genet.* **12**, E3849–E3858 (2016).
8. Avila, F. W., Sirot, L. K., Laflamme, B. A., Rubinstein, C. D. & Wolfner, M. F. Insect seminal fluid proteins: Identification and function. *Annu. Rev. Entomol.* **56**, 21-40 (2011).
9. Chen, P. S. *et al.* A male accessory gland peptide that regulates reproductive behavior of female D. melanogaster. *Cell* **54**, 291–298 (1988).
10. Peng, J. *et al.* Gradual release of sperm bound sex-peptide controls female postmating behavior in Drosophila. *Curr. Biol.* **15**, 207–213 (2005).
11. Jang, Y. H., Chae, H. S. & Kim, Y. J. Female-specific myoinhibitory peptide neurons regulate mating receptivity in Drosophila melanogaster. *Nat. Commun.* **8**, 1–12 (2017).
12. Feng, K., Palfreyman, M. T., Häsemeyer, M., Talsma, A. & Dickson, B. J. Ascending SAG neurons control sexual receptivity of Drosophila females. *Neuron* **83**, 135–148 (2014).
13. Wang, K. *et al.* Neural circuit mechanisms of sexual receptivity in Drosophila females. *Nature* **589**, 577–581 (2021).
14. Wang, F. *et al.* Neural circuitry linking mating and egg laying in Drosophila females. *Nature* **579**, 101–105 (2020).
15. Walker, S. J., Corrales-Carvajal, V. M. & Ribeiro, C. Postmating circuitry modulates salt taste processing to increase reproductive output in Drosophila. *Curr. Biol.* **25**, 2621–2630 (2015).
16. Garbe, D. S. *et al.* Changes in female Drosophila sleep following mating are mediated by SPSN-SAG neurons. *J. Biol. Rhythms* **31**, 551–567 (2016).
17. Kramer, S. J. *et al.* Identification of an allatostatin from the tobacco hornworm Manduca sexta. *Proc. Natl. Acad. Sci. U. S. A.* **88**, 9458–9462 (1991).
18. Wang, C., Zhang, J., Tobe, S. S. & Bendena, W. G. Defining the contribution of select neuropeptides and their receptors in regulating sesquiterpenoid biosynthesis by Drosophila melanogaster ring gland/corpus allatum through RNAi analysis. *Gen. Comp. Endocrinol.* **176**, 347–353 (2012).
19. Zhang, C. *et al.* The neuropeptide allatostatin C from clock-associated DN1p neurons generates the circadian rhythm for oogenesis. *Proc. Natl. Acad. Sci. U. S. A.* **118**, (2021).

20. Johns, D. & Marx, R. Inducible genetic suppression of neuronal excitability. *J. Neurosci.* **19**, 1691–1697 (1999).
21. Kitamoto, T. Conditional modification of behavior in Drosophila by targeted expression of a temperature-sensitive shibire allele in defined neurons. *J. Neurobiol.* **47**, 81–92 (2001).
22. Luan, H., Peabody, N. C., Vinson, C. R. R. & White, B. H. Refined spatial manipulation of neuronal function by combinatorial restriction of transgene expression. *Neuron* **52**, 425-436 (2006).
23. Gao, Q. & Finkelstein, R. Targeting gene expression to the head: The Drosophila orthodenticle gene is a direct target of the Bicoid morphogen. *Development* **125**, 4185–4193 (1998).
24. Asahina, K. *et al.* Tachykinin-expressing neurons control male-specific aggressive arousal in drosophila. *Cell* **156**, 221–235 (2014).
25. Gao, X. J. *et al.* A transcriptional reporter of intracellular Ca 2+ in Drosophila. *Nat. Neurosci.* **18**, 917–925 (2015).
26. Nicolaï, L. J. J. *et al.* Genetically encoded dendritic marker sheds light on neuronal connectivity in Drosophila. *Proc. Natl. Acad. Sci. U. S. A.* **107**, 20553–20558 (2010).
27. Zhang, Y. Q., Rodesch, C. K. & Broadie, K. Living synaptic vesicle marker: Synaptotagmin-GFP. *Genesis* **34**, 142–145 (2002).
28. Fichelson, P., Brigui, A. & Pichaud, F. Orthodenticle and Kruppel homolog 1 regulate Drosophila photoreceptor maturation. *Proc. Natl. Acad. Sci. U. S. A.* **109**, 7893–7898 (2012).
29. Kreienkamp, H. J. *et al.* Functional annotation of two orphan G-protein-coupled receptors, drostar1 and -2, from Drosophila melanogaster and their ligands by reverse pharmacology. *J. Biol. Chem.* **277**, 39937–39943 (2002).
30. Kondo, S. *et al.* Neurochemical Organization of the Drosophila brain visualized by endogenously tagged neurotransmitter receptors. *Cell Rep.* **30**, 284-297.e5 (2020).
31. Wijesekera, T. P., Saurabh, S. & Dauwalder, B. Juvenile hormone is required in adult males for drosophila courtship. *PLoS One* **11**, (2016).
32. de Velasco, B. *et al.* Specification and development of the pars intercerebralis and pars lateralis, neuroendocrine command centers in the Drosophila brain. *Dev. Biol.* **302**, 309–323 (2007).
33. Shiga, S. Anatomy and functions of brain neurosecretory cells in diptera. *Microsc. Res. Tech.* **62**, 114–131 (2003).
34. Jia, D., Xu, Q., Xie, Q., Mio, W. & Deng, W. M. Automatic stage identification of Drosophila egg chamber based on DAPI images. *Sci. Rep.* **6**, 1–12 (2016).
35. Talay, M. *et al.* Transsynaptic mapping of second-order taste neurons in flies by trans-Tango. *Neuron* **96**, 783-795.e4 (2017).
36. Postlethwait, J. H. & Shirk, P. D. Genetic and endocrine regulation of vitellogenesis in Drosophila. *Integr. Comp. Biol.* **21**, 687-700 (1981).
37. Bownes, M. The roles of juvenile hormone, ecdysone and the ovary in the control of Drosophila vitellogenesis. *J. Insect Physiol.* **35**, 409–413 (1989).

38. Bownes, M. & Rembold, H. The titre of juvenile hormone during the pupal and adult stages of the life cycle of Drosophila melanogaster. *Eur. J. Biochem.* **164**, 709–712 (1987).
39. Sugime, Y. *et al.* Upregulation of juvenile hormone titers in female Drosophila melanogaster through mating experiences and host food occupied by eggs and larvae. *Zoolog. Sci.* **34**, 52–57 (2017).
40. Areiza, M., Nouzova, M., Rivera-Perez, C. & Noriega, F. G. Ecdysis triggering hormone ensures proper timing of juvenile hormone biosynthesis in pharate adult mosquitoes. *Insect Biochem. Mol. Biol.* **54**, 98–105 (2014).
41. Meiselman, M. *et al.* Endocrine network essential for reproductive success in Drosophila melanogaster. *Proc. Natl. Acad. Sci. U. S. A.* **114**, E3849–E3858 (2017).
42. Zitnan, D. & Adams, M. E. Neuroendocrine regulation of ecdysis. in *Insect En*docrinology (ed. Gilbert, L. I. ) 253–309 (Elsevier, 2012).
43. Park, Y., Filippov, V., Gill, S. S. & Adams, M. E. Deletion of the ecdysis-triggering hormone gene leads to lethal ecdysis deficiency. *Development* vol. 129 (2002).
44. Bilen, J., Atallah, J., Azanchi, R., Levine, J. D. & Riddiford, L. M. Regulation of onset of female mating and sex pheromone production by juvenile hormone in Drosophila melanogaster. *Proc. Natl. Acad. Sci. U. S. A.* **110**, 18321–18326 (2013).
45. Markow, T. A. Forced matings in natural populations of Drosophila. *Am. Nat.* **156**, 100–103 (2000).
46. Seeley, C. & Dukas, R. Teneral matings in fruit flies: Male coercion and female response. *Anim. Behav.* **81**, 595–601 (2011).
47. Markow, T. A. The secret lives of Drosophila flies. *Elife* **4**, 1–9 (2015).
48. Moshitzky, P. *et al.* Sex-Peptide Activates juvenile hormone biosynthesis in the Drosophila melanogaster corpus allatum. *Arch. Insect Biochem. Physiol.* **32**, 363–374 (1996).
49. Pilpel, N., Nezer, I., Applebaum, S. W. & Heifetz, Y. Mating-increases trypsin in female Drosophila hemolymph. *Insect Biochem. Mol. Biol.* **38**, 320-330 (2008).
50. Yang, C. hui *et al.* Control of the postmating behavioral switch in Drosophila females by internal sensory neurons. *Neuron* **61**, 519–526 (2009).
51. Häsemeyer, M., Yapici, N., Heberlein, U. & Dickson, B. J. Sensory neurons in the Drosophila genital tract regulate female reproductive behavior. *Neuron* **61**, 511-518 (2009).
52. Hassanien, I. T. E., Grötzner, M., Meyering-Vos, M. & Hoffmann, K. H. Neuropeptides affecting the transfer of juvenile hormones from males to females during mating in Spodoptera frugiperda. *J. Insect Physiol.* **66**, 45–52 (2014).
53. Clifton, M. E., Correa, S., Rivera-Perez, C., Nouzova, M. & Noriega, F. G. Male Aedes aegypti mosquitoes use JH III transferred during copulation to influence previtellogenic ovary physiology and affect the reproductive output of female mosquitoes. J. Insect Physiol. **64**, 40-47 (2014).
54. Bachtel, N. D., Hovsepian, G. A., Nixon, D. F. & Eleftherianos, I. Allatostatin C modulates nociception and immunity in Drosophila. *Sci. Rep.* **8**, 1–11 (2018).

55. Díaz, M. M., Schlichting, M., Abruzzi, K. C., Long, X. & Rosbash, M. Allatostatin-C/AstC-R2 Is a aovel pathway to modulate the circadian activity pattern in Drosophila. *Curr. Biol.* **29**, 13-22.e3 (2019).
56. Peng, J., Zipperlen, P. & Kubli, E. Drosophila sex-peptide stimulates female innate immune system after mating via the Toll and Imd pathways. *Curr. Biol.* **15**, 1690–4 (2005).
57. Domanitskaya, E. V, Liu, H., Chen, S. & Kubli, E. The hydroxyproline motif of male sex peptide elicits the innate immune response in Drosophila females. *FEBS J.* **274**, 5659–68 (2007).
58. Yapici, N., Kim, Y.-J., Ribeiro, C. & Dickson, B. J. A receptor that mediates the post-mating switch in Drosophila reproductive behaviour. *Nature* **451**, 33–37 (2008).
59. Bhattarai, J. P. *et al.* Somatostatin inhibition of gonadotropin-releasing hormone neurons in female and male mice. *Endocrinology* **151**, 3258–3266 (2010).
60. Pintér, E., Helyes, Z. & Szolcsányi, J. Inhibitory effect of somatostatin on inflammation and nociception. *Pharmacology and Therapeutics* vol. 112 440–456 (2006).
61. Reiff, T. *et al.* Endocrine remodelling of the adult intestine sustains reproduction in drosophila. *Elife* **4**, 1–19 (2015).
62. Anton, S. & Gadenne, C. Effect of juvenile hormone on the central nervous processing of sex pheromone in an insect. *Proc. Natl. Acad. Sci. U. S. A.* **96**, 5764–5767 (1999).
63. Shemshedini, L., Lanoue, M. & Wilson, T. G. Evidence for a juvenile hormone receptor involved in protein synthesis in Drosophila melanogaster. *J. Biol. Chem.* **265**, 1913–1918 (1990).
64. Wilson, T. G., DeMoor, S. & Lei, J. Juvenile hormone involvement in Drosophila melanogaster male reproduction as suggested by the Methoprene-tolerant 27 mutant phenotype. *Insect Biochem. Mol. Biol.* **33**, 1167–1175 (2003).
65. Yu, J. Y., Kanai, M. I., Demir, E., Jefferis, G. S. X. E. & Dickson, B. J. Cellular organization of the neural circuit that drives Drosophila courtship behavior. *Curr. Biol.* **20**, 1602–14 (2010).
66. von Philipsborn, A. C. *et al.* Neuronal control of Drosophila courtship song. *Neuron* **69**, 509–522 (2011).
67. Hamada, F. N. *et al.* An internal thermal sensor controlling temperature preference in Drosophila. *Nature* **454**, 217–20 (2008).
68. Liu, H. & Kubli, E. Sex-peptide is the molecular basis of the sperm effect in Drosophila melanogaster. *Proc. Natl. Acad. Sci. U. S. A.* **100**, 9929–33 (2003).
69. Pfeiffer, B. D. *et al.* Refinement of tools for targeted gene expression in Drosophila. *Genetics* **186**, 735–55 (2010).
70. Flatt, T. & Kawecki, T. J. Juvenile hormone as a regulator of the trade-off between reproduction and life span in Drosophila melanogaster. *Evolution (N. Y).* **61**, 1980–1991 (2007).
71. Hampel, S. *et al.* Drosophila Brainbow: A recombinase-based fluorescence labeling technique to subdivide neural expression patterns. *Nat. Methods* **8**, 253–259 (2011).
72. Kwak, S. J. *et al.* Drosophila adiponectin receptor in insulin producing cells regulates glucose and lipid metabolism by controlling insulin secretion. *PLoS One* **8**, 2–11 (2013).

73. Schneider, C. A., Rasband, W. S. & Eliceiri, K. W. NIH Image to ImageJ: 25 years of image analysis. *Nat. Methods* **9**, 671–675 (2012).
74. Bergot, B. J. Method for quantitative determination of the four known juvenile hormones in insect tissue using gas chromatography-mass spectroscopy. *J. Chromatogr.* 23–244 (1981).
75. Rivera-Perez, C., Nouzova, M. & Noriega, F. G. A quantitative assay for the juvenile hormones and their precursors using fluorescent tags. *PLoS One* **7**, e43784 (2012).

# Figures

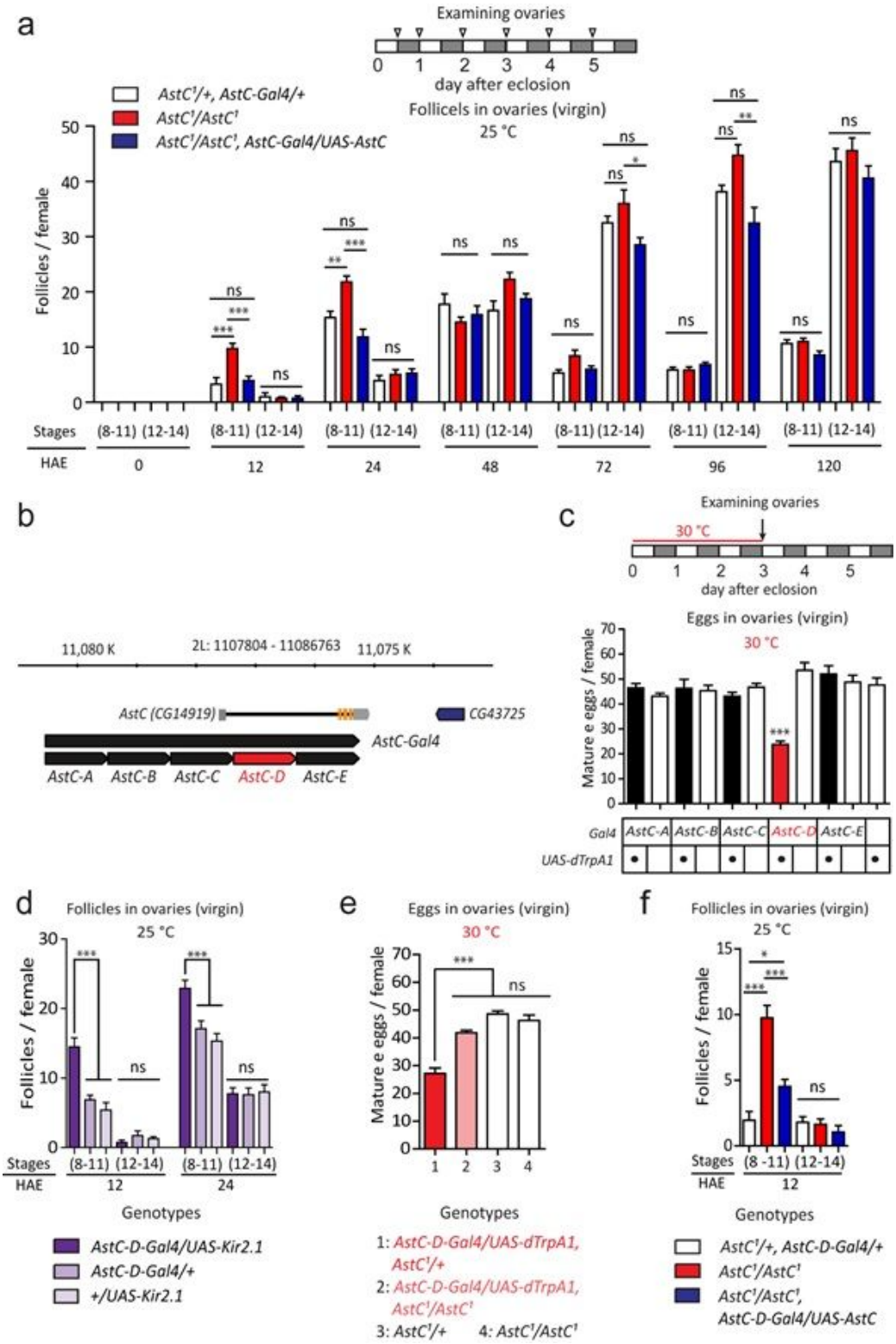


## Figure 1

AstC from AstC-D-Gal4 neurons gates vitellogenesis during reproductive maturation. a Above, experimental protocol for a, d, and f. Below, number of stage 8-11 and 12-14 follicles per virgin female of the indicated genotypes at the indicated hours after eclosion (HAE) (n = 8–12). One-way ANOVA followed by Tukey's test for multiple comparisons (a, d, e, and f); ***p < 0.001; **p < 0.005; ns (non-significance) p > 0.05. b AstC gene structure and genomic fragments (black or red bars) used to generate AstC-Gal4 and

the other related Gal4, Gal4AD, and Gal4DBD transgenes. c Above, experimental protocol for c and e. Below, number of mature eggs per virgin female 3 days after eclosion of the indicated genotypes at 30°C (n = 40–60). Unpaired t-test; ***p < 0.001 compared with Gal4 control (white bar); no labeling, p > 0.05. d Number of stage 8–11 and 12–14 follicles per virgin female of the indicated genotypes at the indicated HAE (n = 8–12). e Number of mature eggs per virgin female of the indicated genotypes 3 days after eclosion at 30°C (n = 40–60). f Number of stage 8–11 and 12–14 follicles per virgin female of the indicated genotypes at 12 HAE (n = 8–12).

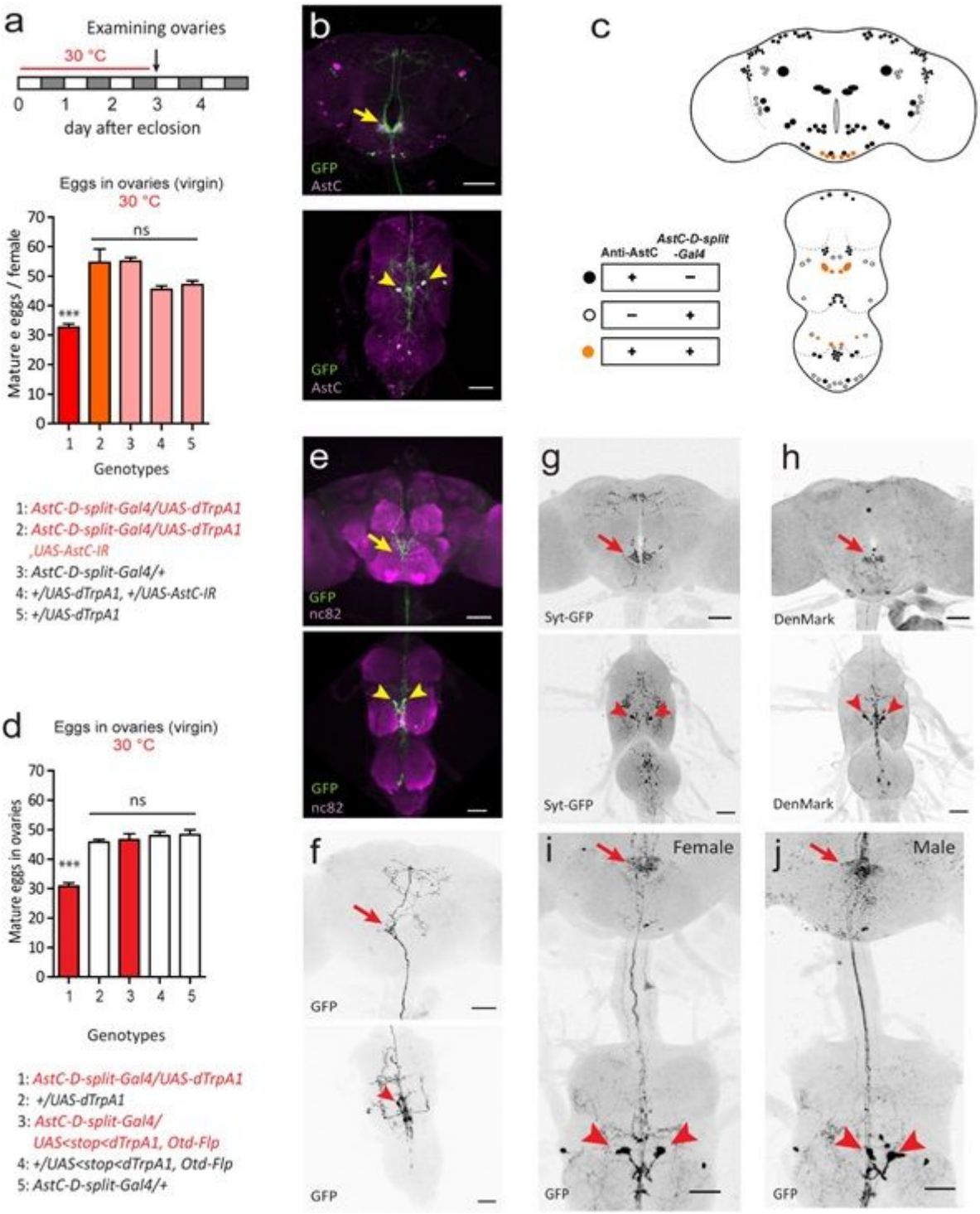


**Figure 2**

Identification and characterization of AstC-mTh neurons. a, d Above, experimental protocol for a and d. Bottom, number of mature eggs per virgin female of the indicated genotypes 3 days after eclosion at 30°C (n = 30–40). One-way ANOVA followed by Tukey's test for multiple comparisons (a and d); ***$p < 0.001$ for comparisons against other groups (genotypes 2–5 for a and d); ns (non-significance) $p > 0.05$. b Confocal Z-projection images of the brain (above) and VNC (bottom) of 4-day-old virgin females carrying AstC-D-split-Gal4 and UAS-mCD8-EGFP stained with anti-AstC (magenta) and anti-GFP (green). Arrowheads indicate two evident neurons in the VNC that project into the dorsal region of the SEZ (yellow arrow). Scale bars, 50 μm. c A schematic indicating anti-AstC and AstC-D-split-Gal4-positive neurons (orange circles), AstC-D-split-Gal4-positive neurons lacking anti-AstC (open circles), and anti-AstC neurons lacking AstC-D-split-Gal4 activity (closed circles). e Confocal Z-projection images of the brain (upper) and VNC (lower) of 4-day-old virgin females carrying AstC-D-split-Gal4 and TRIC transgenes (i.e., UAS-mCD8::RFP, LexAop2-mCD8::GFP; nSyb-MKII::nlsLexADBD;UAS-p65AD::CaM) stained with nc82 antibody (magenta) and anti-GFP (green). TRIC labels two AstC-mTh neuron somas in the VNC (arrowheads) that project into the dorsal region of the SEZ (yellow arrow). Scale bars, 50 μm. f Negative images of TRIC labelling (anti-GFP) of single AstC-mTh neuron in the brain CNS of 4-day-old virgin females, indicating intracellular $Ca2+$ transients, TRIC driven by AstC-D-split-Gal4 labeled one of two AstC-mTh neurons. Arrow indicates SEZ region. Arrowheads (red) indicate AstC-mTh neuron somas. Scale bars, 50 μm. g Negative images of the brain (above) and VNC (bottom) of 4-day-old virgin females carrying AstC-D-split-Gal4 and UAS-Syt-EGFP stained with anti-GFP. Presynaptic domains labeled by Syt-EGFP are evident in the dorsal SEZ region (arrow). Arrowheads indicate AstC-mTh neuron somas. Scale bars, 50 μm. h Negative images of the brain (above) and VNC (bottom) of 4-day-old virgin females carrying AstC-D-split-Gal4 and UAS-DenMark stained with anti-RFP. Postsynaptic domains labeled by DenMark are evident in the dorsal SEZ region (arrow) and AstC-mTh neuron somas (arrowheads). Scale bars, 50 μm. i, j Negative images of the CNS of 4-day-old virgin female (i) and male (j) carrying AstC-D-split-Gal4 and UAS-myr-EGFP stained with anti-GFP. Arrow indicates SEZ region. Arrowheads indicate AstC-mTh neuron somas. Scale bars, 50 μm.

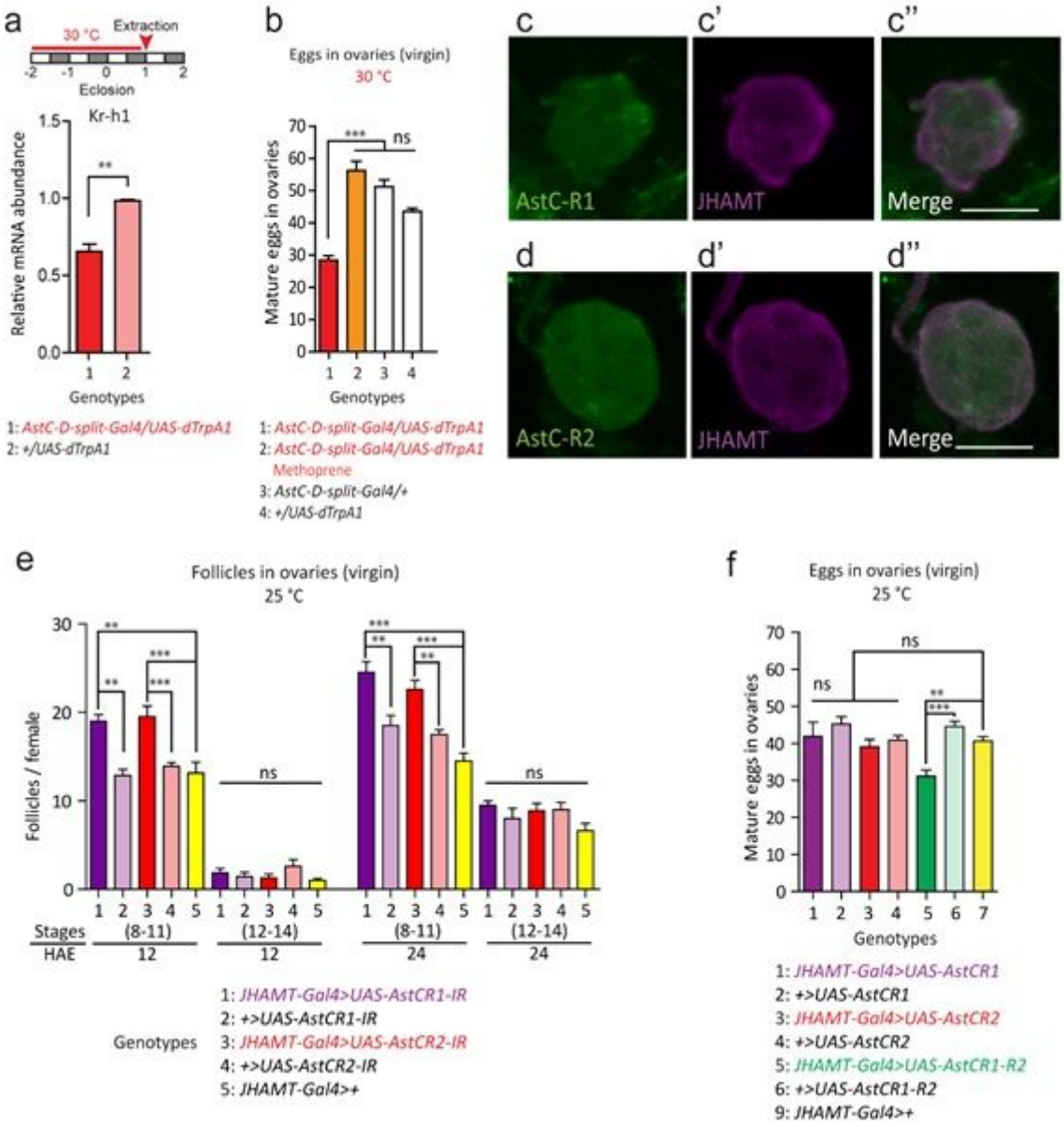


## Figure 3

AstC-mTh neurons regulate JH biosynthesis via AstC-R1 and AstC-R2 in the CA. a Above, experimental protocol. Below, Kr-h1 transcript levels in adult females of the indicated genotypes maintained for 3 days post-eclosion at 30°C. Unpaired t-tests; **p < 0.005. b Number of mature eggs per virgin female of the indicated genotypes 3 days post-eclosion at 30°C (n = 20–40). Genotype 2 was fed methoprene while the others were fed the vehicle control. ANOVA followed by Tukey's test for multiple comparisons (b, e, and f); ***p < 0.001; **p < 0.005; ns (non-significance) p > 0.05. c, d The CA of 4-day-old virgin females carrying AstC-R1-Gal4 (c) or AstC-R2-Gal4 (d) and UAS-mCD8-EGFP stained with anti-JHAMT (magenta) and anti-GFP (green). Scale bars, 25 μm. e Number of stage 8–11 and 12–14 follicles per virgin female of the indicated genotypes at the indicated number of hours after eclosion (HAE) (n = 10–12). f Number of mature eggs per virgin female of the indicated genotypes 3 days post-eclosion at 25°C (n = 40–60).

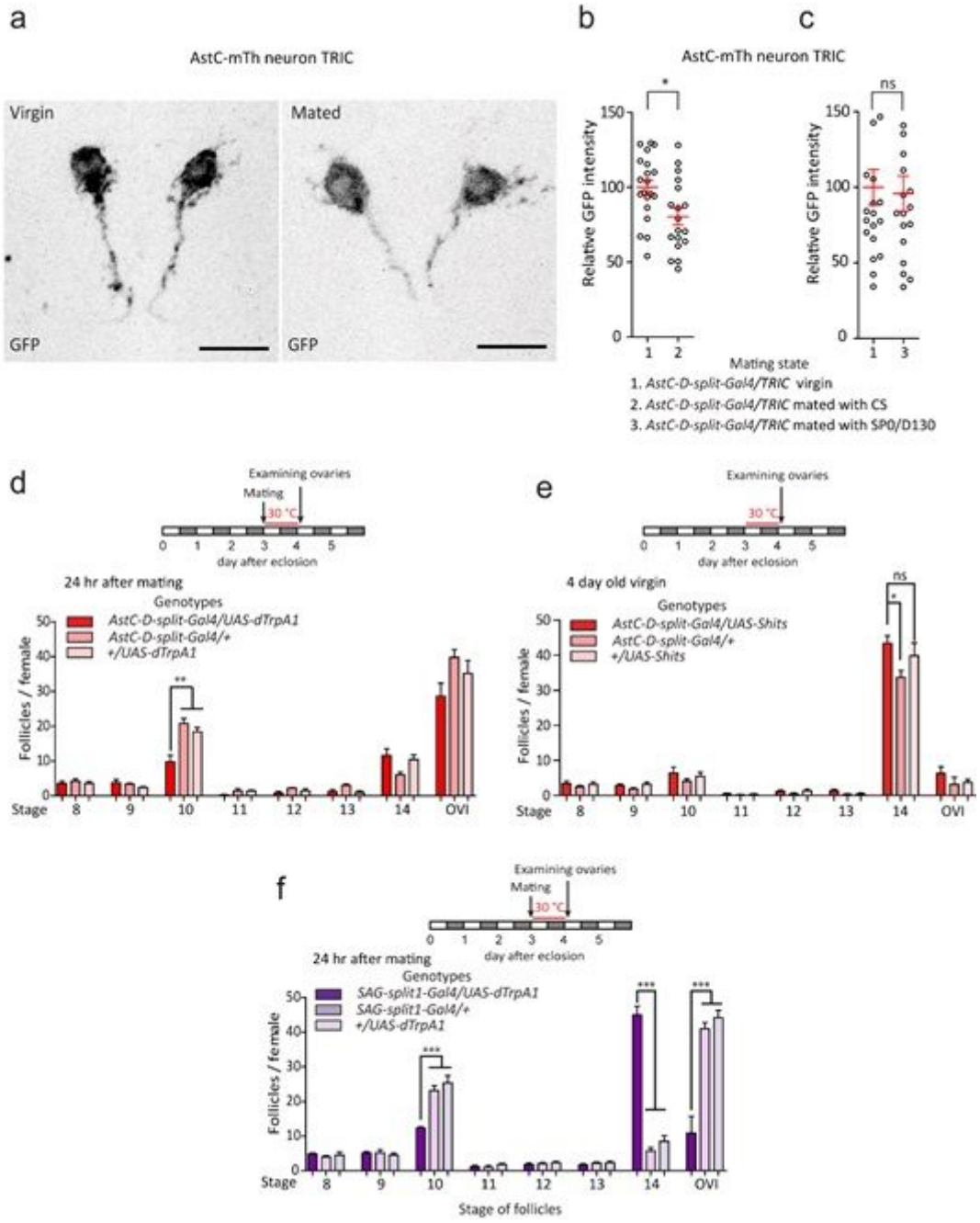


## Figure 4

AstC-mTh neurons gate mating-induced vitellogenesis in response to SP. a Negative images of TRIC labelling in AstC-mTh neurons of virgin (left) and mated (right) females carrying AstC-D-split-Gal4 and TRIC transgenes, indicating intracellular Ca2+ transients. Scale bars, 10 μm. b, c GFP intensities from TRIC-expressing AstC-mTh neurons of virgin females and females mated with control Canton-S (CS) (b) or SP0/D130 (c) males. Unpaired t-tests; *p < 0.05. ns (non-significance) and no labeling, p > 0.05. d, e, f Above, experimental protocol. Number of follicles of the indicated stage and oviposited eggs (OVI) from females of the indicated genotypes 24 hours after mating (n = 6–10 for each genotype). One-way ANOVA followed by Tukey's test for multiple comparisons among genotypes; ***p < 0.001; **p < 0.005; *p < 0.05; ns (non-significance) and no labeling, p > 0.05.

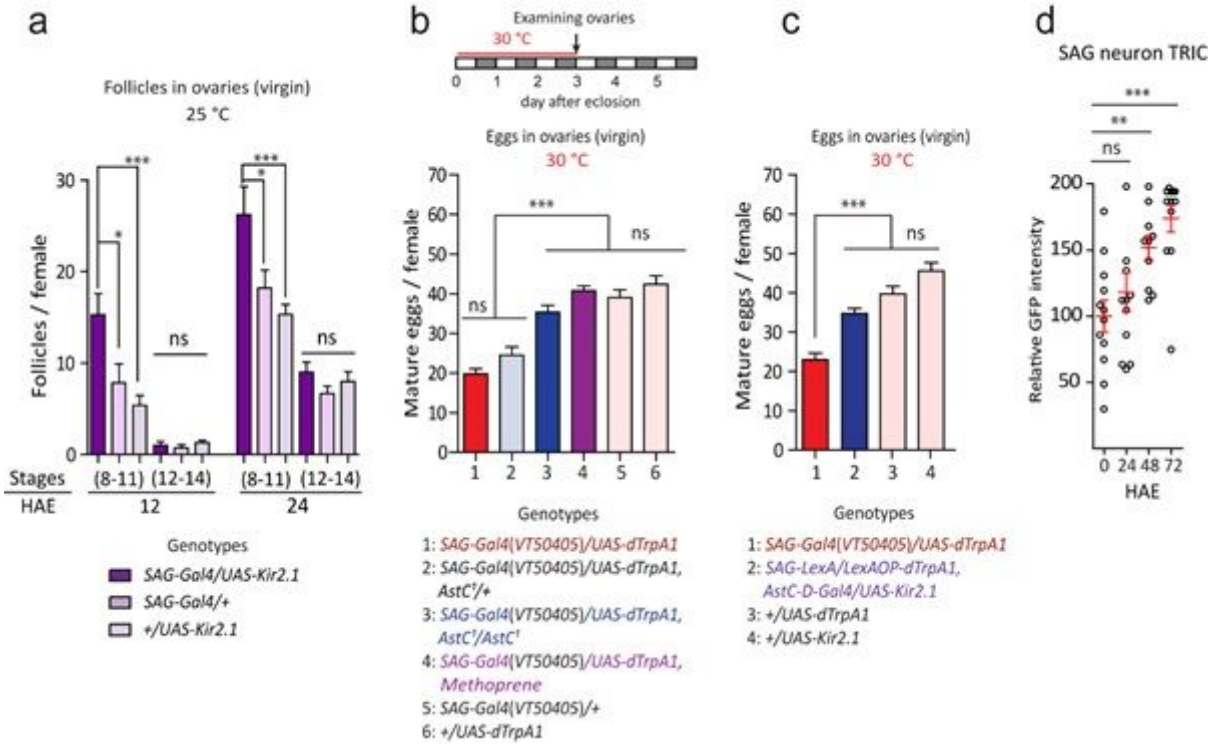


**Figure 5**

SAG neurons function upstream of AstC-mTh neurons and gate vitellogenesis during reproductive maturation. a Number of stage 8–11 and 12–14 follicles per virgin female of the indicated genotypes at the indicated hours after eclosion (HAE) (n = 8–12 for each genotype). One-way ANOVA followed by Tukey's test for multiple comparisons (a-d); ***p < 0.001; **p < 0.005; *p < 0.05; ns (non-significance) p > 0.05. b, c Above, experimental protocol for b and c. Number of mature eggs per virgin female of the indicated genotypes 3 days after eclosion under 30°C (n = 40–60 for each genotype). d GFP intensities from SAG neurons of TRIC virgin females show Ca2+ activity at the indicated hours after eclosion (HAE).

# Supplementary Files

This is a list of supplementary files associated with this preprint. Click to download.

- Supplementalinformation.docx